Electronic Supplementary Information

Hierarchically porous doped carbons fabricated by the strategy of ion transfer coordination (ITC)

Zhi Xu [a], Le Li [a], Chenhong Fang [a], Linjuan Zhang [b,*] and Guyu Xiao [a,*]

[a] Shanghai Key Laboratory of Electrical Insulation and Thermal Ageing, School of Chemistry and Chemical Engineering, State Key Laboratory of Metal Matrix Composites, Shanghai Jiao Tong University, Shanghai 200240, P. R. China
[b] Key Laboratory of Interfacial Physics and Technology, Shanghai Institute of Applied Physics, Chinese Academy of Sciences, Shanghai 201800, P. R. China

*E-mail: zhanglinjuan@sinap.ac.cn, gyxiao@sjtu.edu.cn

1. Experimental Section

1.1 Sample Preparation

Chemicals: 2-Methylimidazole, zinc nitrate hexahydrate ($Zn(NO_3)_2 \cdot 6H_2O$), ferric nitrate nonahydrate ($Fe(NO_3)_3 \cdot 9H_2O$), methanol, dopamine hydrochloride, and ammonium hydroxide solution (NH_4OH, 28–30%) were purchased from Adamas Reagent and used without further purification.

Synthesis of ZIF-8: 2-Methylimidazole (1.31 g) and $Zn(NO_3)_2 \cdot 6H_2O$ (1.13 g) were dissolved in 50 mL of methanol, respectively. Then, both solutions were mixed and stirred at room temperature for 24 h. ZIF-8 with a size of 120 nm was obtained by centrifugation, washing with methanol for several times, and drying at 60 °C in a vacuum oven. Similarly, ZIF-8 with a size of 60 and 30 nm were prepared by using 200 and 400 mL of methanol, respectively.

Synthesis of PDA nanobubbles: 30 mg of ZIF-8 was dispersed in 30 mL of methanol. Then, 100 mg of dopamine hydrochloride was added into the above dispersion. Afterwards, 0.25 mL of ammonium hydroxide solution was added into the above mixture and then stirred at room temperature for 24 h. The products were collected via centrifugation, washing with methanol for several times, and drying at 60 °C *in vacuo*.

Synthesis of ZIF-8@PDA: The synthesis of ZIF-8@PDA was similar to that of PDA nanobubbles, except that the reaction time was reduced to several hours. The ZIF-8 templates within ZIF-8@PDA composites were etched completely after 24 h.

Synthesis of NCNB-1: The PDA nanobubbles templated by ZIF-8 of 120 nm were pyrolyzed under N_2 atmosphere at 950 °C for 3 h to prepare NCNB-1.

Synthesis of NCNB-2 and NCNB-3: The synthesis of NCNB-2 and NCNB-3 was similar to that of NCNB-1, except that the ZIF-8 crystals with a size of 60 and 30 nm replace the ones with a size of 120 nm, respectively.

Synthesis of NCNB-4: The PDA nanobubbles, prepared by using ZIF-8 of 30 nm as template, were pyrolyzed under N_2 atmosphere at 400 °C for 3 h, then treated with 0.1 M HCl solution to remove the Zn-containing species and washed with excess deionized water. This

intermediate carbonized product is name iNCNB-4. Subsequently, iNCNB-4 was subjected to the second heat treatment at 950 $^\circ$C for 3 h under N_2 atmosphere to form NCNB-4.

Synthesis of Fe-doped ZIF-8 (ZIF-Fe): The synthesis of ZIF-Fe was similar to that of the ZIF-8 with a size of 30 nm, except that additional 33.3 mg of $Fe(NO_3)_3 \cdot 9H_2O$ was added in the course of reaction.

Synthesis of Zn^{+2}/Fe^{+3}-coordinated PDA nanobubbles: The synthesis process of Zn^{+2}/Fe^{+3}-coordinated PDA nanobubbles was similar to that of the PDA nanobubbles, except that ZIF-8 was replaced with ZIF-Fe.

Synthesis of Fe-doped carbon nanobubbles (NCNB-Fe): The Zn^{+2}/Fe^{+3}-coordinated PDA nanobubbles were pyrolyzed at 950 $^\circ$C for 3 h under N_2 atmosphere to generate NCNB-Fe.

1.2 Material Characterization

Transmission electron microscopy (TEM) was performed on a Tecnai G2 Spirit Biotwin at 120 kV. HAADF-STEM image and element mapping were obtained on a Talos F200X apparatus at 200 kV. Aberration-corrected HAADF-STEM observations were performed on a JEM-ARM200F instrument at 200 kV with cold filed-emission gun and aberration corrector. Fe K-edge X-ray absorption spectroscopy (XAS) were measured at beamline 14W1 of the Shanghai Synchrotron Radiation Facility (SSRF), China. Data were obtained using a Si (111) double crystal monochromator in fluorescent mode. X-ray diffraction (XRD) was carried out using a Bruker D8 advance polyfunctional X-Ray diffractometer, equipped with Cu Kα (λ = 1.5418 Å) radiation. Raman spectroscopy was conducted on a DXR Raman Microscope excited by a laser beam of 532 nm. Nitrogen adsorption/desorption isotherms were measured on an Autosorb-iQA3200-4 sorption analyzer instrument at 77 K. Mercury intrusion porosimetry measurements were performed on a Micromeritics AutoPore IV 9500 system. X-ray photoelectron spectroscopy (XPS) analysis was conducted on an AXIS Ultra DLD system with an Al Kα achromatic X-ray source.

1.3 Electrochemical Measurements

Electrochemical measurements were performed on a CHI760E electrochemical workstation with a three-electrode system, using the glassy carbon rotating disk electrode/rotating ring disk electrode (RDE/RRDE), Ag/AgCl electrode, and Pt wire as the working electrode,

reference electrode, and counter electrode, respectively. For the preparation of the working electrode, 4 mg of catalyst was dispersed into the mixture of 490 μL of ethanol and 10 μL of 5 wt% Nafion under ultrasonication to make a well-dispersed suspension. The loading of as-made catalysts is 0.6 mg cm^{-2}. The Pt/C catalyst with a loading of 0.1 mg cm^{-2} was compared in the same conditions. The RDE and RRDE tests were performed using linear sweep voltammetry (LSV) at a scan rate of 10 mV s^{-1} in the potential window of 0–1.2 V (vs. RHE) in O$_2$-saturated 0.1 M KOH or 0.1 M HClO$_4$ solution with a rotation speed of 1600 rpm[1].

The electron transfer number (n) and H$_2$O$_2$ yield were calculated from RRDE results by the following equations[2]:

$$n = 4 \times \frac{i_d}{i_r/N + i_d}$$

$$H_2O_2\% = 200 \times \frac{i_r/N}{i_r/N + i_d}$$

Where i_d is the disk current, i_r is the ring current, and N is the collection efficiency of the ring current ($N = 0.37$).

The stability was assessed by cycling test between 0.6 and 1.0 V at 200 mV s^{-1} in O$_2$-saturated electrolyte, and two LSV curves were recorded before and after continuous 5,000 CV cycles. The methanol tolerance was measured by chronoamperometry with the addition of 20 mL methanol into O$_2$-saturated electrolyte at the 200th second.

The electrochemical active surface area (ECSA) of the catalysts is calculated by the electrochemical double-layer capacitance (C_{dl}). The ECSA is measured on the RDE working electrode, which is calculated by the double-layer charging from the CV curves at various scan rates in non-Faradaic potential region.[3] The potential range is 1.05–1.15 V (vs. RHE). The scan rates are 2, 4, 6, 8, 10, and 12 mV s^{-1}, respectivity. There is a linear relationship between the charging current and scan rate, and the correponding slope is C_{dl}.[3] The C_{dl} and ECSA obey the following equation: ECSA = $(C_{dl}/C_s)A_{geo}$, where C_s (0.04 mF cm^{-2}) and A_{geo} (0.07 cm^2) is the specific capacitance and geometric area of the glassy-carbon electrode, respectively.[3]

1.4 Performances of carbons in Zn-air batteries

The performances of the as-made carbons were further characterized by the home-made Zn-air batteries. Typically, the catalyst coated on a gas diffusion layer with a loading of 1.0 mg

cm^{-2} was employed as an air-cathode electrode, the polished Zn foil was used as the anode electrode, and 6 M KOH containing 0.2 M ZnCl$_2$ was utilized as the electrolyte. The galvanostatic discharge/charge cycling was conducted at a current density of 10 mA cm^{-2} with a discharge/charge time of 5 min.

2. Figures and Tables
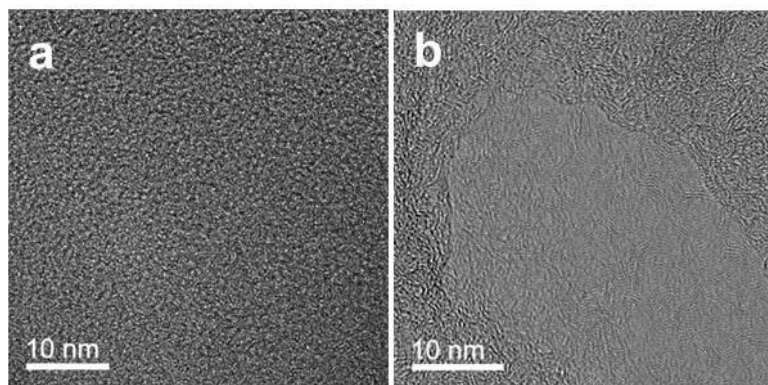
Fig. S1 HR-TEM images of (a) the PDA nanobubble and (b) NCNB-1.
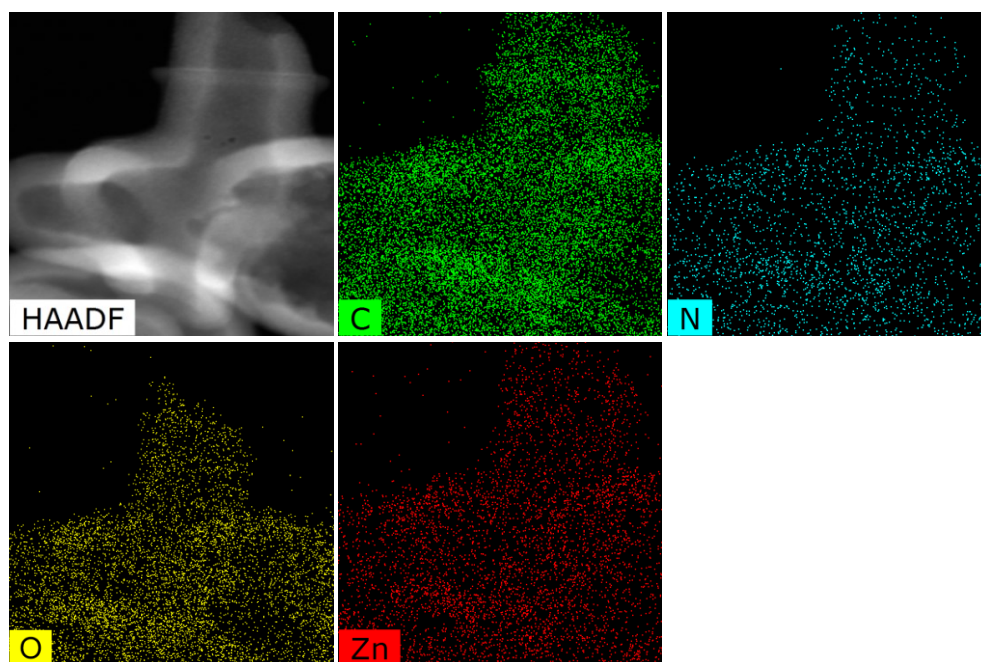
Fig. S2 HAADF-STEM image and element mappings of the (Zn^{+2}-coordinated) PDA nanobubbles.
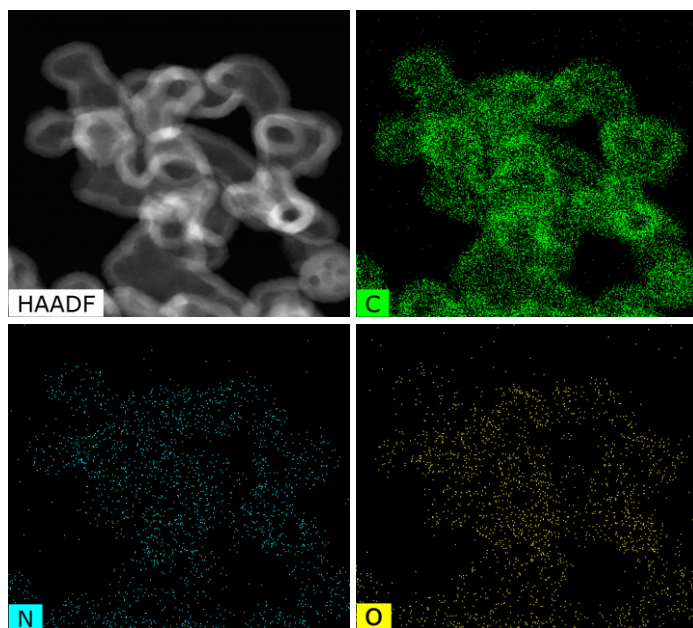
Fig. S3 HAADF-STEM image and element mappings of NCNB-1.
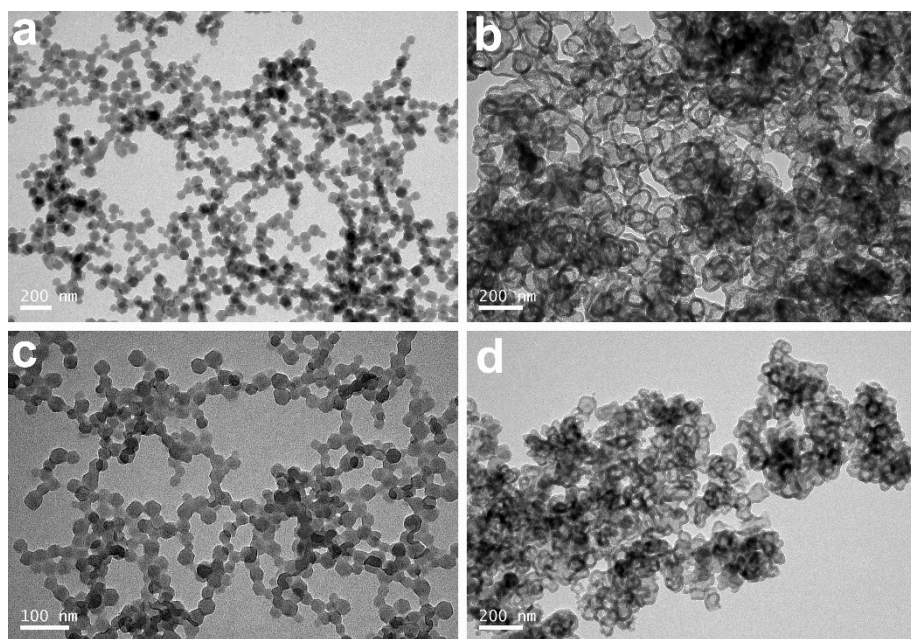
Fig. S4 TEM images of (a) ZIF-8 with a size of 60 nm, (b) NCNB-2, (c) ZIF-8 with a size of 30 nm, and (d) NCNB-3.
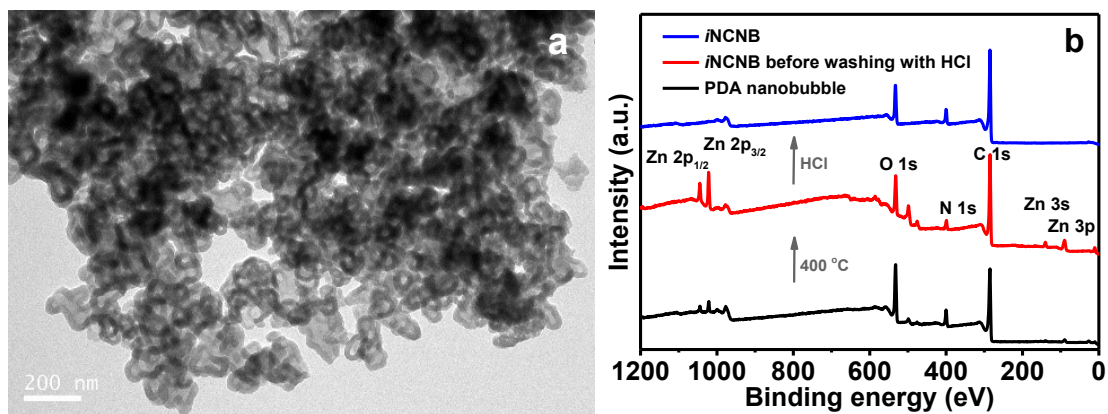
Fig. S5 (a) TEM image of NCNB-4, (b) XPS survey spectra.
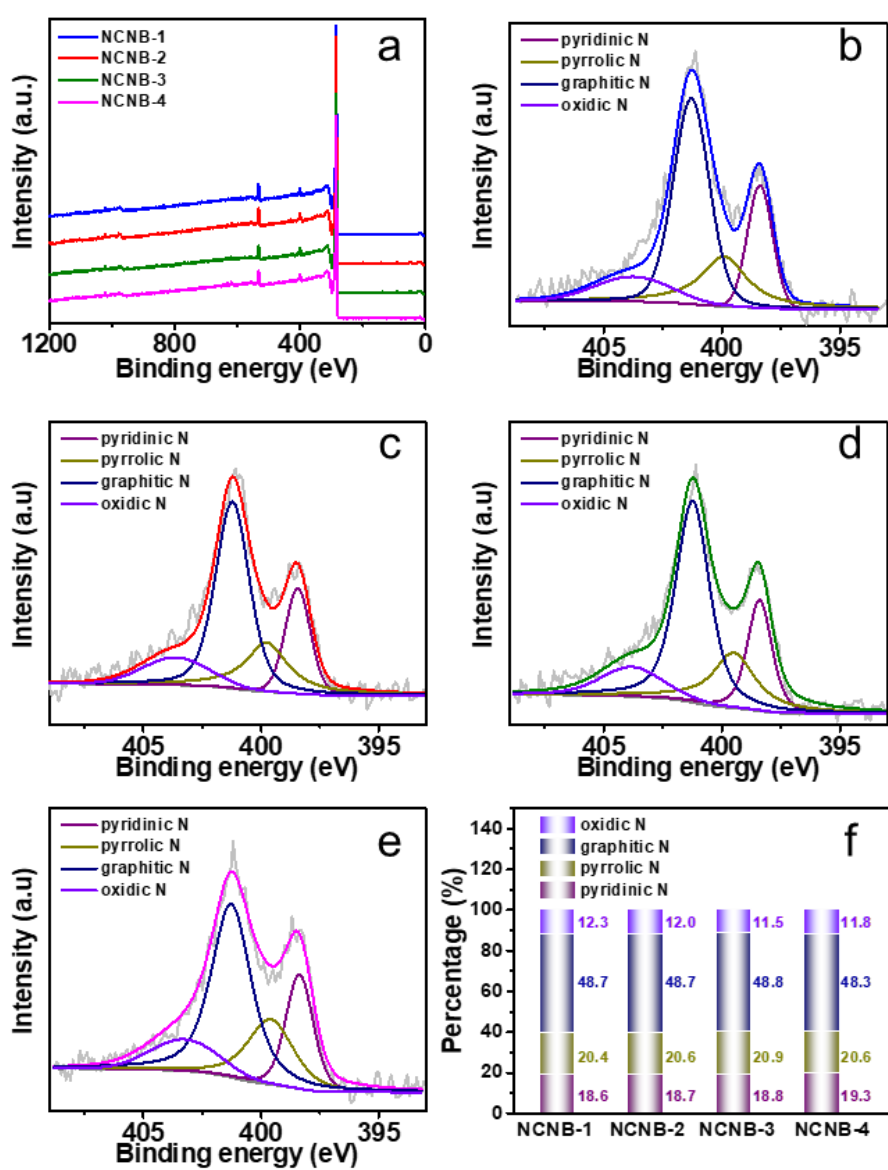
Fig. S6 (a) XPS survey spectra of NCNBs. (b–e) High-resolution N 1s XPS spectra of (b) NCNB-1, (c) NCNB-2, (d) NCNB-3, and (e) NCNB-4. (f) Percentage of various nitrogen species.
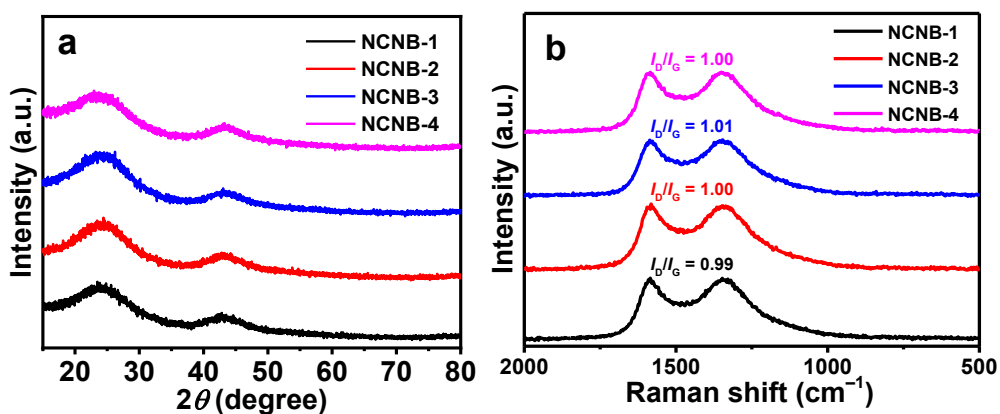
Fig. S7 (a) XRD patterns and (b) Raman spectra of NCNBs.
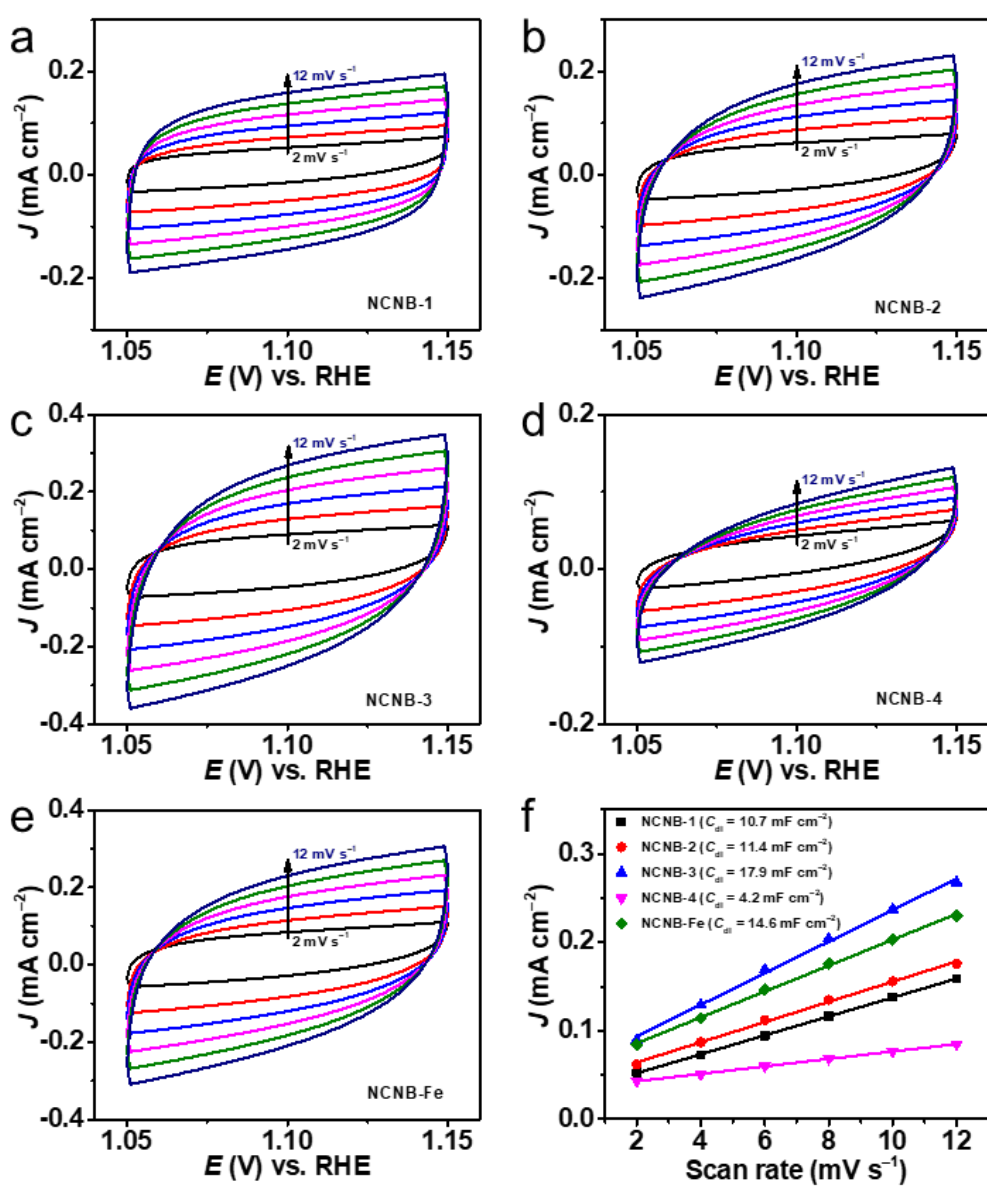
Fig. S8 (a–e) CV curves of NCNBs in the double layer region at a scan rate of 2, 4, 6, 8, 10, and 12 mV s^{-1} in 0.1 M KOH, and (f) capacitive current derived from CV curves at 1.10 V as a function of scan rate.
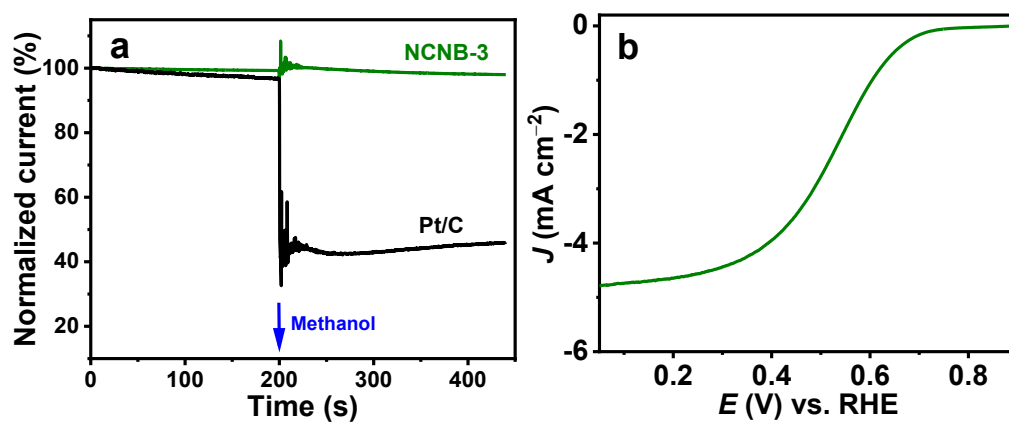
Fig. S9 (a) Chronoamperometric response to methanol for NCNB-3 in 0.1 M KOH solution. (b) LSV curve of NCNB-3 in 0.1 M HClO$_4$.
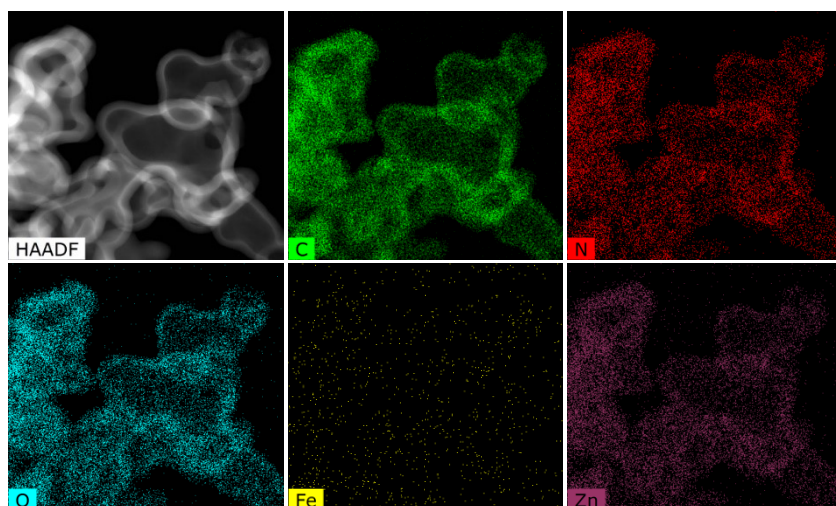
Fig. S10 HAADF-STEM image and element mappings of the Zn^{+2}/Fe^{+3}-coordinated PDA nanobubbles.
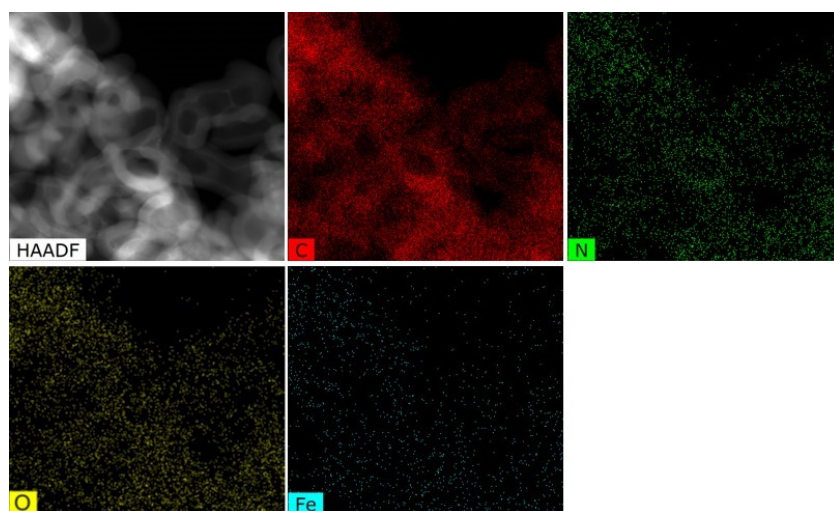
Fig. S11 HAADF-STEM image and element mappings of NCNB-Fe.
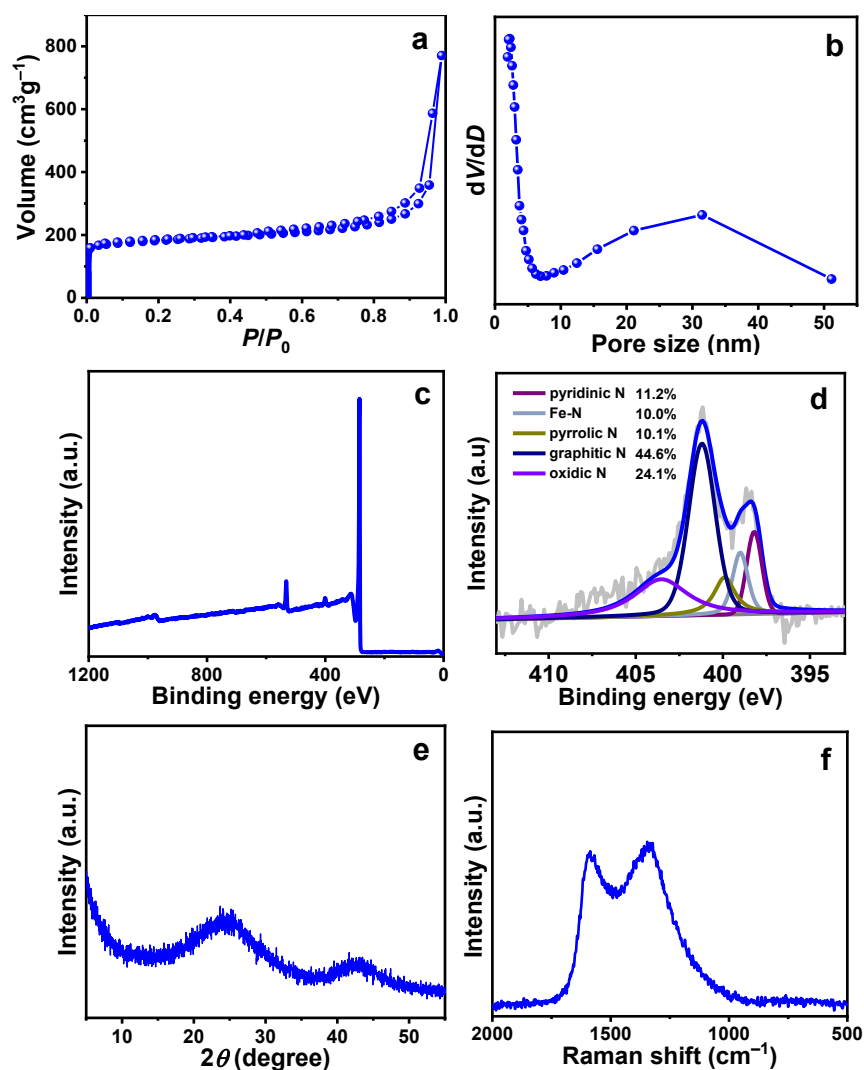
Fig. S12 (a) N_2 adsorption/desorption isotherms, (b) BJH pore-diameter distribution, (c) XPS survey spectrum, (d) high-resolution N 1s XPS spectrum, (e) XRD pattern, and (f) Raman spectrum of NCNB-Fe.
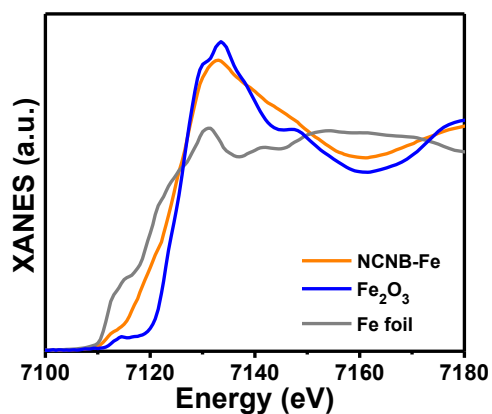
Fig. S13 XANES spectra at the Fe K-edge of NCNB-Fe, Fe_2O_3, and Fe foil.
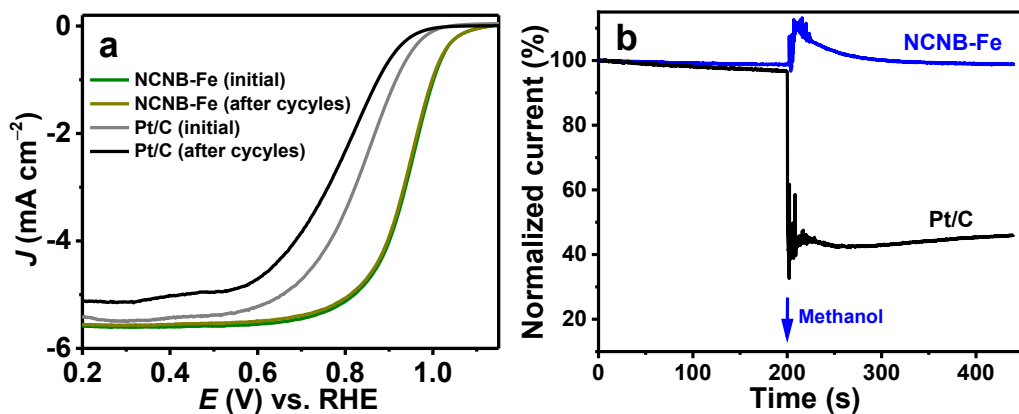
Fig. S14 (a) LSV curves before and after 5,000 cycles and (b) chronoamperometric response to methanol for NCNB-Fe and Pt/C in 0.1 M KOH solution.
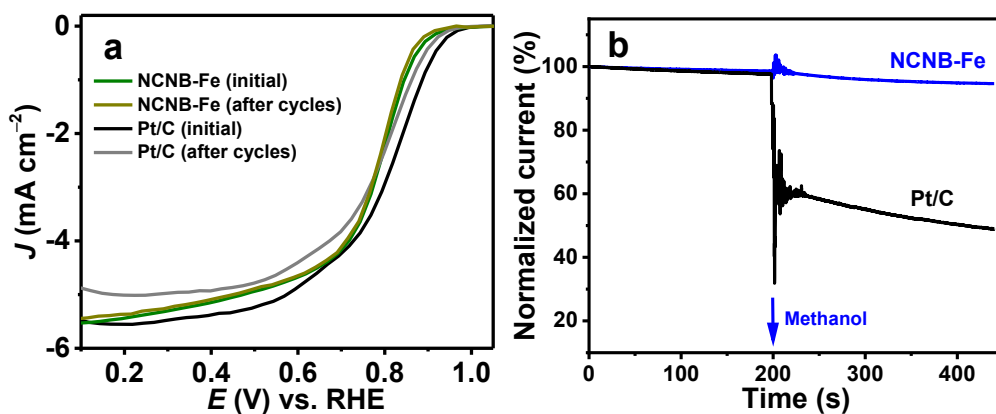
Fig. S15 (a) LSV curves before and after 5,000 cycles and (b) chronoamperometric response to methanol for NCNB-Fe and Pt/C in 0.1 M HClO$_4$ solution.
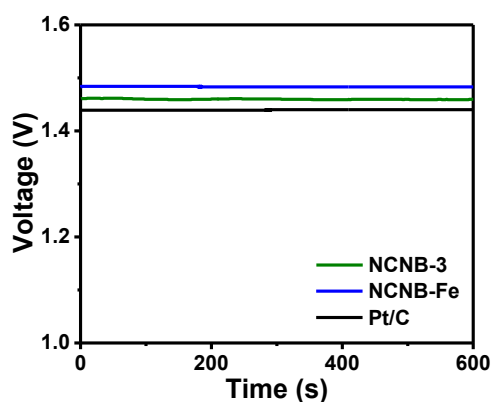
Fig. S16 Open circuit potential of the NCNB-3, NCNB-Fe, and Pt/C based Zn-air batteries.

Table S1 Pore-structure parameters of NCNBs and NCNB-Fe.

Sample	S_{BET}[a] ($m^2\,g^{-1}$)	S_{micro}[b] ($m^2\,g^{-1}$)	V_{total}[c] ($cm^3\,g^{-1}$)	V_{micro}[d] ($cm^3\,g^{-1}$)
NCNB-1	518	370	0.99	0.19
NCNB-2	525	407	1.01	0.21
NCNB-3	553	427	1.23	0.22
NCNB-4	421	320	0.96	0.16
NCNB-Fe	545	426	1.16	0.22

[a] Specific surface area is calculated from N_2 adsorption/desorption isotherms. [b] Specific surface area of micropores are calculated by the V–T plot method. [c] Total pore volume is calculated from N_2 adsorption/desorption isotherms. [d] Pore volume of micropores are calculated via the V–T plot method.

Table S2 Element contents of NCNBs and NCNB-Fe calculated by XPS results.

Sample	C	N	O	Fe
	(wt%)			
NCNB-1	93.93	2.67	3.40	/
NCNB-2	93.22	2.95	3.83	/
NCNB-3	94.47	2.60	2.93	/
NCNB-4	93.65	2.59	3.76	/
NCNB-Fe	93.07	2.55	3.50	0.88

Table S3 Catalytic activity of NCNB-3 and metal-free doped carbons for ORR in 0.1 M KOH.

Catalyst	E_{onset} (V)	$E_{1/2}$ (V)	J_L ($mA\,cm^{-2}$)	Reference
Carbon plates	0.94	0.835	5.36	*Adv. Mater.* 2018, 30, 1803588[4]
B,N-doped carbon	0.98	0.84	~5.5	*Adv. Sci.* 2018, 5, 1800036[5]
Biomass carbon	0.96	0.825	4.3	*Energy Environ. Sci.* 2019, 12, 648[6]
Modified fullerene	0.911	0.833	5.29	*Angew. Chem. Int. Ed.* 2019, 58, 3859[7]
Porous carbon plates	0.988	0.85	5.7	*Adv. Mater.* 2019, 31, 1900341[8]
SCNS	0.85	0.770	5.05	*Angew. Chem. Int. Ed.* 2020, 59, 19627[9]
Pt/C	0.94	0.836	5.43	This work
NCNB-3	**0.95**	**0.856**	**5.49**	**This work**

Table S4 Catalytic activity of NCNB-Fe and single-atom doped carbons for ORR in 0.1 M KOH.

Catalyst	E_{onset} (V)	$E_{1/2}$ (V)	J_L (mA cm^{-2})	Reference
Co-SAs@NC	0.96	0.82	4.96	*Angew. Chem. Int. Ed.* 2019, 58, 5359[10]
Fe-ISA/SNC	/	0.896	5.5	*Adv. Mater.* 2018, 30, 1800588[11]
SA-Fe/NG	/	0.88	~5.8	*PNAS*, 2018, 115, 6626[12]
Fe-N-C HNSs	1.046	0.87	5.9	*Adv. Mater.* 2019, 31, 1806312[13]
Fe-N/P-C-700	0.941	0.867	5.66	*J. Am. Chem. Soc.* 2020, 142, 2404[14]
FeN$_3$S	0.94	0.86	~5.7	*ACS Energy Lett.* 2021, 6, 379[15]
Fe$_1$-HNC	0.93	0.842	5.8	*Adv. Mater.* 2020, *32*, 1906905[16]
Pt/C	0.94	0.836	5.43	This work
NCNB-Fe	**1.05**	**0.940**	**5.60**	**This work**

Table S5 Catalytic activity of NCNB-Fe and single-atom doped carbons for ORR in 0.1 M HClO$_4$.

Catalyst	E_{onset} (V)	$E_{1/2}$ (V)	J_L (mA cm^{-2})	Reference
CoNC700	0.89	0.73	5.2	*Small* 2018, 14, 1704319[17]
FeSAs/PTF-600	0.89	0.74	~5.2	*ACS Energy Lett.* 2018, 3, 833[18]
up-Fe-N-CNFs	0.81	0.68	~5.0	*Energy Enviorn. Sci.* 2018, 11, 2208[19]
p-Fe-N-CNFs	0.84	0.74	5.5	*Energy Enviorn. Sci.* 2018, 11, 2208[19]
Cr/N/C-950	/	0.761	~5.3	*Angew. Chem. Int. Ed.* 2019, 58, 12469[20]
Fe$_{0.5}$-N-C	0.87	0.76	5.4	*J. Am. Chem. Soc.* 2019, 141, 2035[21]
Zn-N-C-1	/	0.746	4.6	*Angew. Chem. Int. Ed.* 2019, 58, 7035[22]
Pt/C	0.94	0.810	5.45	This work
NCNB-Fe	**0.90**	**0.792**	**5.30**	**This work**

Table S6 Performances of the Zn-air batteries with NCNB-Fe and metal-free or single-atom doped carbons as air-cathode catalysts.

Catalyst	loading (mg cm^{-2})	specific capacity (mAh g^{-1})	peak power density (mW cm^{-2})	Reference
NPMC-1000	0.5	835 (@5mA cm^{-2}) 695 (@25mA cm^{-2})	55	*Nat. Nanotech.* 2015, 10, 444[23]
Si-N-C-6	0.9	990 (@20 mA cm^{-2})	100	*Nano Energy* 2019, 62, 700[24]
NPCS-900	1.5	848 (@2 mA cm^{-2}) 656 (@20 mA cm^{-2})	79	*Nano Energy* 2019, 60, 536[25]
NSC-1000	2.0	581 (@100 mA cm^{-2})	167.8	*Nano Energy* 2019, 59, 207[26]
Co-SAs@NC	1.75	897 (@20 mA cm^{-2})	105	*Angew. Chem. Int. Ed.* 2019, 58, 5359[10]
Fe-N/P-C	3	~665 (@100 mA cm^{-2})	133	*J. Am. Chem. Soc.* 2020, 142, 2404[14]
CoNi-SAs	1.4	886 (@20 mA cm^{-2})	101	*Adv. Mater.* 2019, 31, 1905622.[27]
Fe-N$_x$-C	/	~770 (@10 mA cm^{-2})	96	*Adv Funct. Mater.* 2019, 29, 1808872[28]
Pt/C	1.0	713 (@10 mA cm^{-2})	128	This work
NCNB-3	**1.0**	**763 (@10 mA cm^{-2})**	**151**	**This work**
NCNB-Fe	**1.0**	**801 (@10 mA cm^{-2})**	**188**	**This work**

References

[1]   L. Jiao, G. Wan, R. Zhang, H. Zhou, S.-H. Yu, H.-L. Jiang, *Angew. Chem. Int. Ed.* 2018, *57*, 8525.

[2]   J. Sun, S. E. Lowe, L. Zhang, Y. Wang, K. Pang, Y. Wang, Y. Zhong, P. Liu, K. Zhao, Z. Tang, H. Zhao, *Angew. Chem. Int. Ed.* 2018, *57*, 16511.

[3]   Y.-L. Wu, X. Li, Y.-S. Wei, Z. Fu, W. Wei, X.-T. Wu, Q.-L. Zhu, Q. Xu, *Adv. Mater.*, 2021, *33*, 2006965.

[4]   J. Han, G. Huang, Z. Wang, Z. Lu, J. Du, H. Kashani, M. Chen, *Adv. Mater.* 2018, *30*, 1803588.

[5]   T. Sun, J. Wang, C. Qiu, X. Ling, B. Tian, W. Chen, C. Su, *Adv. Sci.* 2018, *5*, 1800036.

[6]   X. Li, B.Y. Guan, S. Gao, X. W. Lou, *Energy Environ. Sci.* 2019, *12*, 648.

[7]   J. Zhu, Y. Huang, W. Mei, C. Zhao, C. Zhang, J. Zhang, I. S. Amiinu, S. Mu, *Angew. Chem. Int. Ed.* 2019, *58*, 3859.

[8]   X. Peng, L. Zhang, Z. Chen, L. Zhong, D. Zhao, X. Chi, X. Zhao, L. Li, X. Lu, K. Leng, C. Liu, W. Liu, W. Tang, K. P. Loh, *Adv. Mater.* 2019, *31*, 1900341.

[9]   L. Zou, C. C. Hou, Q. Wang, Y. S. Wei, Z. Liu, J. S. Qin, H. Pang, Q. Xu, *Angew. Chem. Int. Ed.* 2020, *59*, 19627.

[10]   X. Han, X. Ling, Y. Wang, T. Ma, C. Zhong, W. Hu, Y. Deng, *Angew. Chem. Int. Ed.* 2019, *58*, 5359.

[11]   Q. Li, W. Chen, H. Xiao, Y. Gong, Z. Li, L. Zheng, X. Zheng, W. Yan, W. C. Cheong, R. Shen, N. Fu, L. Gu, Z. Zhuang, C. Chen, D. Wang, Q. Peng, J. Li, Y. Li, *Adv. Mater.* 2018, *30*, 1800588.

[12]   L. Yang, D. Cheng, H. Xu, X. Zeng, X. Wan, J. Shui, Z. Xiang, D. Cao, *Proc. Natl. Acad. Sci.* 2018, *115*, 6626.

[13]   Y. Chen, Z. Li, Y. Zhu, D. Sun, X. Liu, L. Xu, Y. Tang, *Adv. Mater.* 2019, *31*, 1806312.

[14]   K. Yuan, D. Lutzenkirchen-Hecht, L. Li, L. Shuai, Y. Li, R. Cao, M. Qiu, X. Zhuang, M. K. H. Leung, Y. Chen, U. Scherf, *J. Am. Chem. Soc.* 2020, *142*, 2404.

[15]   M. Wang, W. Yang, X. Li, Y. Xu, L. Zheng, C. Su, B. Liu, *ACS Energy Lett.* 2021, *6*, 379.

[16]   X. Zhang, S. Zhang, Y. Yang, L. Wang, Z. Mu, H. Zhu, X. Zhu, H. Xing, H. Xia, B. Huang, J. Li, S. Guo, E. Wang, *Adv. Mater.* 2020, *32*, 1906905.

[17]   G. Wan, P. Yu, H. Chen, J. Wen, C. Sun, H. Zhou, N. Zhang, Q. Li, W. Zhao, B. Xie, T. Li, J. Shi, *Small* 2018, *14*, 1704319.

[18] J.-D. Yi, R. Xu, Q. Wu, T. Zhang, K.-T. Zang, J. Luo, Y.-L. Liang, Y.-B. Huang, R. Cao, *ACS Energy Lett.* 2018, *3*, 883.

[19] B.-C. Hu, Z.-Y. Wu, S.-Q. Chu, H.-W. Zhu, H.-W. Liang, J. Zhang, S.-H. Yu, *Energy Environ. Sci.* 2018, *11*, 2208.

[20] E. Luo, H. Zhang, X. Wang, L. Gao, L. Gong, T. Zhao, Z. Jin, J. Ge, Z. Jiang, C. Liu, W. Xing, *Angew. Chem. Int. Ed.* 2019, *58*, 12469.

[21] S. H. Lee, J. Kim, D. Y. Chung, J. M. Yoo, H. S. Lee, M. J. Kim, B. S. Mun, S. G. Kwon, Y.-E. Sung, T. Hyeon, *J. Am. Chem. Soc.* 2019, *141*, 2035.

[22] J. Li, S. G. Chen, N. Yang, M. G. Deng, S. Ibraheem, J. H. Deng, J. Li, L. Li, Z. D. Wei, *Angew. Chem. Int. Ed.* 2019, *58*, 7035.

[23] J. Zhang, Z. Zhao, Z. Xia, L. Dai, *Nat. Nanotech.* 2015, *10*, 444.

[24] Q. Wei, M. Cherif, G. Zhang, A. Almesrati, J. Chen, M. Wu, N. Komba, Y. Hu, T. Regier, T.-K. Sham, F. Vidal, S. Sun, *Nano Energy* 2019, *62*, 700.

[25] S. Chen, L. Zhao, J. Ma, Y. Wang, L. Dai, J. Zhang, *Nano Energy* 2019, *60*, 536.

[26] K. Yuan, C. Lu, S. Sfaelou, X. Liao, X. Zhuang, Y. Chen, U. Scherf, X. Feng, *Nano Energy* 2019, *59*, 207.

[27] X. Han, X. Ling, D. Yu, D. Xie, L. Li, S. Peng, C. Zhong, N. Zhao, Y. Deng, W. Hu, *Adv. Mater.* 2019, *31*, 1905622.

[28] J. X. Han, X. Y. Meng, L. Lu, J. J. Bian, Z. P. Li, C. W. Sun, *Adv. Funct. Mater.* 2019, *29*, 1808872.